URSI GASS 2023, Sapporo, Japan, 19 – 26 August 2023

Modelling the Ionospheric Alfvén Resonator Harmonic Frequency Separation at Eskdalemuir, UK

R. M. Hodnett*(1), T. K. Yeoman(1), C. D. Beggan(2) and D. M. Wright(1)
(1) University of Leicester, Leicester, UK; rmh38@leicester.ac.uk
(2) British Geological Survey, Edinburgh, UK

Abstract

Ionospheric Alfvén Resonances (IAR) have been observed in Eskdalemuir induction coil magnetometer data. In order to investigate the harmonic frequency separation, we have modelled the IAR using magnetic field strength and plasma mass density. We have used three models of electron density; the IRI, E-CHAIM and an adjusted IRI model using ionosonde data. We find that the IRI and E-CHAIM models perform best.

1 Introduction

Ionospheric Alfvén Resonances (IAR) occur when Alfvén waves propagating along Earth's magnetic field lines are partially reflected at boundaries in the ionosphere where the Alfvén velocity gradient meets a maximum. These boundaries are located where there are sharp changes in the plasma mass density, which are near the bottom of the ionosphere and above the F-region peak. The Alfvén waves resonate in this ionospheric cavity and hence an IAR is formed [1].

IAR appear in dynamic spectrograms as discrete spectral bands as the IAR have multiple harmonics, usually during the nighttime. The harmonic frequency separation (Δf) is used to describe the IAR frequencies, rather than the fundamental, which is often not visible in spectrograms.

IAR were first observed at mid-latitude [2] and have since been observed across of range of latitudes, including in induction coil magnetometer data at Eskdalemuir Magnetic Observatory, UK. Generally Δf is expected to increase from dusk to midnight, as the plasma mass density decreases and Alfvén velocity decreases. Δf then decreases towards dawn. However, at Eskdalemuir more unusual variations in the frequencies have been observed [3].

We have modelled the IAR Δf at Eskdalemuir to investigate the behaviour of the IAR for years 2013–2021.

2 Data

Eskdalemuir Magnetic Observatory is a British Geological Survey site in which two induction coil magnetometers (channel 1 orientated north–south and channel 2 orientated east–west) are situated, located at a geomagnetic latitude of 57.5°N and a geomagnetic longitude of 83.3°E.

We have analysed the IAR Δf the data set for the complete years of 2013 – 2021 and obtained Δf values for this time period. We used the channel 2 magnetometer data as the IAR are more visible in these spectrograms. To find Δf, we first used a u-net [4] which has been developed to identify IAR harmonics from spectrograms [5]. From these output images we automatically extracted Δf by computing the average distance between the peaks of the harmonics, resulting in 16 Δf values per hour, for times where IAR are detected. The was done each day for the time range of 18:00 - 08:00 UT as IAR are a nighttime phenomena. We found that the u-net detected IAR more often during the autumn months and least during the winter months. It should be noted that during the winter the IAR harmonics appear more diffuse in the spectrograms and so are harder for the u-net to detect.

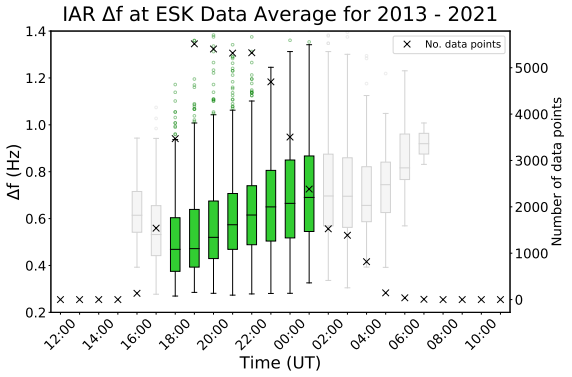

Figure 1. Hourly average Δf data as boxplots for Eskdalemuir 2013–2021. UT is on the x-axis and Δf on the left y-axis, which has a limit of 1.4 Hz. The right y-axis shows thw number of data points, which are plotted as black crosses. The horizontal black line across each bin corresponds to the median Δf for that UT. The lower and upper boundaries of each box are the first and third quartiles of the frequencies, and the whiskers being 1.5 times the interquartile range. Circular points show outliers. UTs that have significant data points are shaded green, which are those that have more points than the standard deviation of the hourly binned data points (here greater than 2090 points).

The Δf values we obtained from this method are displayed

in Figure 1, which shows a boxplot for each hour across the full data set. When no IAR is detected, a data point is omitted. The green shaded bins correlate to times where the number of data points is greater than the standard deviation of the hourly binned data points, hence there are enough data points at those UTs to perform analysis on.

3 Modelling

To model the IAR Δf at Eskdalemuir we performed a time of flight (T_f) calculation for the Alfvén waves to travel up and down the ionospheric cavity, where $\Delta f = 1/T_f$ [6]. The time of flight is related to the Alfvén velocity (V_A) as follows:

$$T_f = 2\int_a^b 1/V_A \mathrm{d}l \tag{1}$$

$$V_A = \frac{B}{\sqrt{\mu_0 \rho}} \tag{2}$$

where B is the magnetic field strength, ρ is the plasma mass density and μ_0 is the permeability of free space. The integral limits a and b are the bottom and top boundaries of the IAR cavity.

The ionospheric plasma mass density changes with altitude and so we modelled Alfvén velocity profiles with velocities every 10 km. We used percentage ion compositions and electron densities from the International Reference Ionosphere (IRI) to model ρ profiles, by assuming quasi-neutrality. The IRI is a model which is based on ionospheric, magnetic and solar parameters. The IRI models the nighttime ionosphere in the altitude range of 80–2000 km which we have used as the size of the resonator cavity. When modelling Alfvén velocity above the F2-region peak, the velocities reach a maximum and so have minimal effect on Δf, as follows from Equation 1. This also applies towards the bottom of the ionosphere. We modelled a ρ profile for every hour during 2013–2021.

To model B we used the International Geomagnetic Reference Field (IGRF–13). We considered the of angle the magnetic field line, where $\tan\theta$ is given by Equation 3 and B_x, B_y and B_z are the components of the total magnetic field. We interpolated over the magnetic field and found values to correspond with the 10 km increments of the IRI, including the $1/\cos\theta$ which comes from the curvature of the magnetic field line. We found $1/\cos\theta$ did not vary significantly over this altitude range.

$$\tan\theta = \frac{({B_x}^2 + {B_y}^2)^{1/2}}{B_z} \tag{3}$$

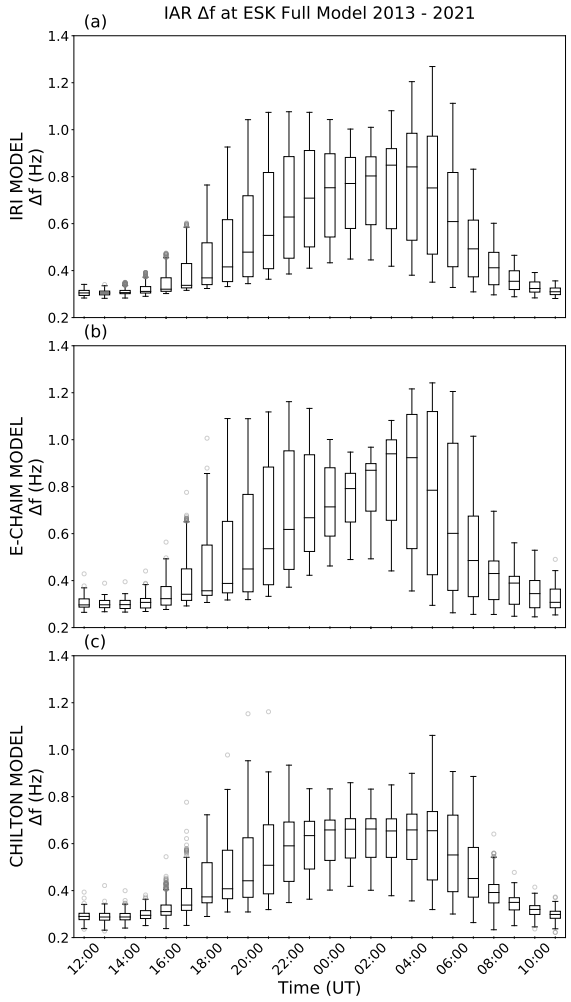

Figure 2. Boxplots of the modelled hourly Δf values for 2013–2021 at Eskdalemuir, for (a) IRI model, (b) E-CHAIM model and (c) Chilton model.

Using Equation 1 we calculated a time of flight for each hour, resulting in a modelled Δf value for each hour. Figure 2(a) is a boxplot of the hourly averages for 2013–2021.

The Alfvén velocity is strongly dependent on the plasma mass density and hence electron density. The Empirical-Canadian High Arctic Ionospheric Model (E-CHAIM) was made to improve models of ionospheric electron density at high latitudes [7, 8, 9]. By scaling the plasma mass density by the E-CHAIM (v3.1.4) electron density profiles instead of those given by the IRI, we modelled Δf as shown by the boxplot in Figure 2(b).

The critical frequency of the ionosphere, $foF2$, is related to peak electron density Ne by $foF2 = 8.98 \times \sqrt{Ne}$. It is useful to compare modelled $foF2$ values with those from data. The closest ionosonde to Eskdalemuir is the Chilton ionosonde, which is located at a latitude of 51.70 °N (3.7 ° south of Eskdalemuir). By comparing the IRI model of $foF2$ at that location and the measured ionosonde data, we modelled another set of electron density profiles by applying the perturbation (Equation 4) between model and data

(Ne_{CHIL}) at Chilton to Eskdalemuir. The resulting adjusted model is shown in Figure 2(c).

$$1 + \frac{Ne_{CHIL} - Ne_{IRI}}{Ne_{IRI}} \tag{4}$$

4 Results and Discussion

In Figures 2(a) and (b), a decrease in Δf can be seen at around 00:00 UT. From our analysis, we found that this feature appears in the models during the winter months. This is likely to be due to a semidiurnal component of $foF2$, which can occur at mid-latitudes [10]. This frequency decrease is not clearly visible in the data, however it may be related to the decrease at 04:00 UT seen in Figure 1. As the u-net did not detect the IAR as often in the winter, there are fewer data points. We plan to investigate this feature in further study.

Reduced versions of the models are shown in Figure 3. Here, modelled Δf values are only included when there is a corresponding data point and so Figure 3 can now be compared directly to Figure 1, which shows the data.

In Figure 4 the percentage difference between the models and the data is plotted. The percentage difference here is defined as 100*((model-data)/data)). The IRI and E-CHAIM models perform similarly, with absolute median percentage differences of 19 % for the IRI model and 20 % for E-CHAIM. The Chilton model has a median percentage difference of 22 %. In general all three models tend to underestimate Δf, which could suggest that they are overestimating electron density or that the time of flight treatment is not fully capturing the nature of the IAR characteristics.

The performance of the models vary across different days. For example, Figure 5 shows two case studies, for 05/03/2013 (a) and 16/09/2014 (b). Δf extracted from the data is plotted in green, with the IRI, E-CHAIM and Chilton models in black, red and blue. On 05/03/2013, the models are slightly underestimating Δf, with the E-CHAIM model performing the best, at an absolute median percentage difference of 15 %. The IRI model has an absolute percentage difference of 21 % and the Chilton model has an absolute percentage difference of 28 %. On 16/09/2014, all models perform better. The Chilton model performs best at 6.4 %, with E-CHAIM at 8.0 % and IRI at 10 %.

5 Conclusion

In general, the models perform well. The Chilton model performs the worst despite being data driven, which may be because the distance between Eskdalemuir and Chilton is too large. However, if the perturbations in the Chilton data are due to phenomena such as Atmospheric Gravity Waves (AGWs), a more thorough analysis would be needed on a case by case basis. There would be a time shift between

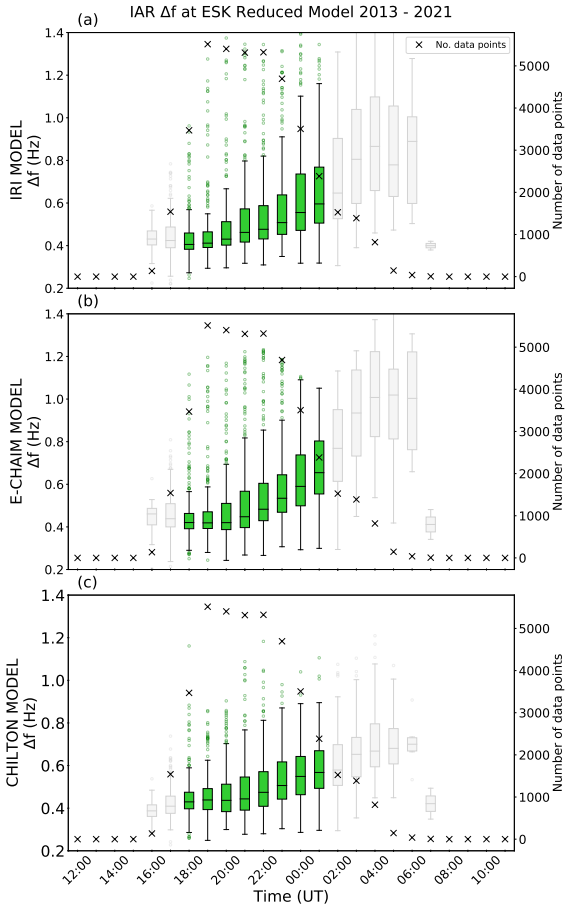

Figure 3. Reduced models for Δf at ESK, for (a) IRI model, (b) E-CHAIM model and (c) Chilton model. The boxplots only include times corresponding where there is data. They are plotted in the same format as Figure 1.

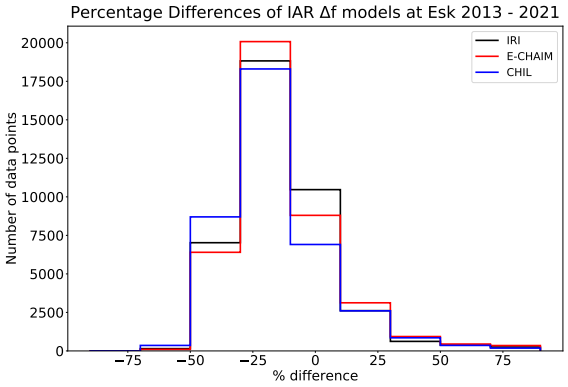

Figure 4. The percentage difference between the models and data. The x-axis has limits of -80 % and 80 %. The IRI model is plotted in black, E-CHAIM in red and Chilton in blue.

AGW related electron density perturbations at Eskdalemuir to those at Chilton, and so this time shift would need to be applied to the model on days where possible AGW activity has been identified.

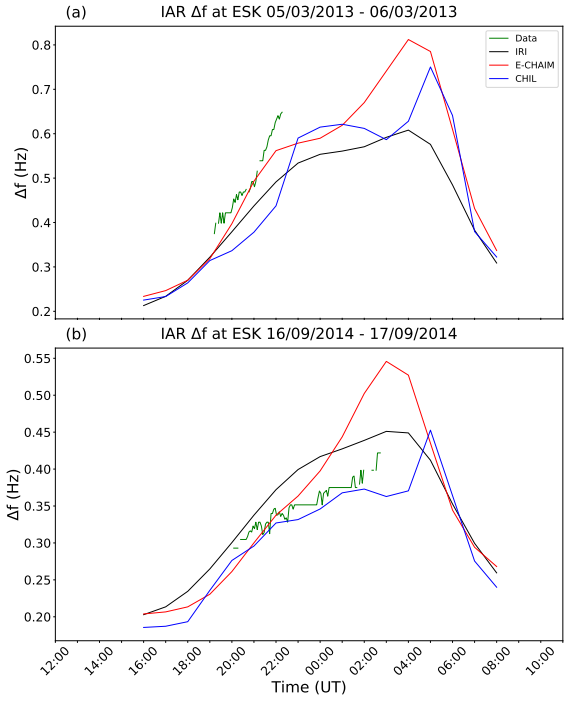

Figure 5. Eskdalemuir Δf from the data (green), IRI model (black), E-CHAIM model (red) and Chilton model (blue), for 05/03/2013 (a) and 16/09/2014 (b). The y-axis shows Δf and the x-axis shows UT time. Modelled values have been plotted from 16:00 - 08:00 UT.

Acknowledgements

R. M. Hodnett is supported by the Central England NERC Training Alliance and is a British Geological Survey BUFI student.

British Geological Survey Eskdalemuir magnetometer data BGS deposited data search, data and sample code available to view.
`webapps.bgs.ac.uk/services/ngdc/accessions/index.html?simpleText=induction%20coil`

International Reference Ionosphere
`irimodel.org/`

International Geomagnetic Reference Field
`www.ngdc.noaa.gov/IAGA/vmod/igrf.html`

E-CHAIM
E-CHAIM is supported under Defence Research and Development Canada contract number W7714-186507/001/SS and is maintained by the Canadian High Arctic Ionospheric Network (CHAIN) with operations support from the Canadian Space Agency.

Chilton ionosonde (RAL Space)
`www.ukssdc.ac.uk/ionosondes/view_latest.html`

References

[1] S. V. Polyakov, "On properties of an ionospheric Alfvén resonator", *KAPG on Solar–Terrestrial Physics, Nauka, Moscow*, **3**, 1976, pp. 72–73.

[2] P. P. Belyaev, C. V. Polyakov, V. O. Rapoport, V. Yu. Trakhtengerts, "Experimental studies of the spectral resonance structure of the atmospheric electromagnetic noise background within the range of short-period geomagnetic pulsations", *Radiophysics and Quantum Electronics*, **32**, 6, 1989, pp. 491–501, doi:10.1007/bf01058169.

[3] C. D. Beggan, and M. Musur, "Observation of Ionospheric Alfvén Resonances at 1-30 Hz and Their Superposition With the Schumann Resonances," *Journal of Geophysical Research: Space Physics*, **123**, 5, May 2018, pp. 4202–4214, doi:10.1029/2018ja025264.

[4] O. Ronneberger, P. Fischer, and T. Brox, "U-Net: Convolutional Networks for Biomedical Image Segmentation", *Lecture Notes in Computer Science*, 2015, pp. 234-241, doi:10.1007/978-3-319-24574-4_28.

[5] P. Marangio, V. Christodoulou, R. Filgueira, H. F. Rogers, and C. D. Beggan, "Automatic Detection of Ionospheric Alfvén Resonances in Magnetic Spectrograms using U-Net", *Computers and Geosciences*, **145**, 104598, 2020, doi:10.1016/j.cageo.2020.104598.

[6] S. V. Polyakov, and V. O. Rapoport, "The ionospheric Alfvén resonator", *Geomagnetism and Aeronomy*, **21**, 1981, pp. 610–614.

[7] D. R. Themens, P. T. Jayachandran, I. Galkin, and C. Hall, "The Empirical Canadian High Arctic Ionospheric Model (E-CHAIM): NmF2 and hmF2", *Journal of Geophysical Research: Space Physics*, **122**, 8, 2017, pp. 9015-9031, doi:10.1002/2017JA024398.

[8] D. R. Themens, P. T. Jayachandran, D. Bilitza et al, "Topside Electron Density Representations for Middle and High Latitudes: A Topside Parameterization for E-CHAIM Based on the NeQuick", *Journal of Geophysical Research: Space Physics*, **123**, 2, 2018, pp. 1603–1617, doi:10.1002/2017ja024817.

[9] D. R. Themens, P. T. Jayachandran, A. M. McCaffrey, B. Reid, R. H. Varney, "A bottomside parameterization for the Empirical Canadian High Artic Ionospheric Model (E-CHAIM)", *Radio Science*, **54**, 5, 2019, pp. 397-414, doi:10.1029/2018rs006748.

[10] N. Zolotukhina, N. Polekh, E. Romanova, and A. Polyakova, "Stability of the seasonal variations in diurnal and semidiurnal components of mid-latitude F2 layer parameters", *Advances in Space Research*, **54**, 3, 2014, pp. 342–354, doi:10.1016/j.asr.2013.11.026.